HIPPOCAMPUS 23:890–902 (2013)

Postnatal Development of *Homer1a* in the Rat Hippocampus

Corinne J. Montes-Rodríguez,* Valérie Lapointe, Vivek Trivedi, Qian Lu, Aubrey M. Demchuk, and Bruce L. McNaughton*

ABSTRACT: ***Homer1a*** **(H1a) is an immediate early gene involved in multiple forms of synaptic plasticity. It exhibits a postnatal increase in the rat forebrain (Brakeman et al. (1997) Nature 386:284-288) and reduces the density and size of dendritic spines in hippocampal neurons (Sala et al. (2003) J Neurosci 23:6327-6337). We evaluated hippocampal H1a expression at different postnatal ages (P3, P5, P7, P9, P15, P19, P23, P35, and adult) using Fluorescence *In Situ* Hybridization (FISH) and qRT-PCR. Maximal electroconvulsive shock (MECS) was used to induce maximal expression relative to home cage (HC) controls. Large scale images and confocal *z*-stacks from dorsal subiculum (DS), CA1, CA3, and dentate gyrus (DG) were analyzed by both manual and automated methods. In DS, CA1, and CA3 a significant proportion of cells (40%) expressed small but detectable levels of H1a from P3; however, MECS did not up-regulate H1a during the first postnatal week. MECS induced H1a positive cells during the second postnatal week and induction reached adult levels at P9. H1a-Intra Nuclear Foci (INF) size and intensity varied with age, increasing at P19-23 in CA1 and CA3 and from P9 to P23 in DS. In DG, H1a expression exhibited a lamination pattern and an H1a-INF size and intensity gradient across the granule cell layer, consistent with the outside-in maturation of DG granule cells. The developmental progression of H1a corresponds to the synaptic refinement period supporting the conclusion that H1a could play an important role in this process. © 2013 Wiley Periodicals, Inc.**

KEY WORDS: **synaptic plasticity; activity dependent; immediate early genes; synaptic maturation; INF-size and intensity; MECS**

INTRODUCTION

The establishment of adult patterns of synaptic connections is a highly dynamic process involving an intrinsic genetic program, experience-dependent plasticity, and spontaneous neuronal activity (McAllister, 2007; Flavell and Greenberg, 2008; Lu et al., 2009). Immediate Early Genes (IEGs) play a crucial role in translating cellular activity into the activation of specific genetic programs involved in the regulation of synaptic efficacy (Kubik et al., 2007). In the developing brain, these programs may underlie the initial self-organization of connectivity, whereas the same plasticity mechanisms may eventually regulate experience-dependent reorganization and learning in the adult (O'Donovan, 1999; Blankenship and Feller, 2009).

Homer1a (H1a) is an IEG involved in multiple forms of synaptic plasticity that is up-regulated in neurons after seizures (Brakeman et al., 1997; Kato et al., 1997) and in the hippocampus during long-term potentiation or after exploration of a novel environment (Vazdarjanova et al., 2002; Vazdarjanova et al., 2004; Marrone et al., 2008). It is necessary for homeostatic scaling (Hu et al., 2010) and regulates calcium homeostasis (Worley et al., 2007). H1a also induces mGluR1 and mGluR5 activity (Ango et al., 2001), regulates activity-induced post and presynaptic structural remodeling (Inoue et al., 2007) and dendritic axonal targeting of mGluR5 (Ango et al., 2000). Moreover, *Homer1* knockout mice exhibit behavioral and glutamatergic abnormalities and a schizophrenia-like phenotype (Lominac et al., 2005; Szumlinski et al., 2005; Jaubert et al., 2007).

Although H1a functions suggest that it may be important during neuronal development, few studies have been done. H1a exhibits a postnatal increase in the rat forebrain (Brakeman et al., 1997) and reduces the density and size of dendritic spines in cultured hippocampal neurons (Sala et al., 2003). In addition, H1a and H1b/c expression in X*enopus* optic tectal neurons causes axon pathfinding and target recognition errors, indicating that the balance between long/constitutive and short/activity-dependent *Homer* forms are crucial for a fine tuning of synaptic connections (Foa et al., 2001).

H1a location at the postsynaptic density (PSD), its functional interrelation with glutamatergic activity, and the requirement of proper Homer protein levels for correct neuronal assembly suggest an important role for H1a expression during postnatal development. On the other hand, the role of IEGs in synaptic plasticity and memory consolidation has been broadly documented in the hippocampus (Guzowski, 2002; Kubik et al., 2007). In this context, we evaluated H1a

Department of Neuroscience, Canadian Centre for Behavioural Neuroscience, The University of Lethbridge, Lethbridge, AB, T1K 3M4, Canada

Grant sponsors: Alberta Innovates-Health Solutions Polaris Award, AI-HS postdoctoral fellowship.

*Correspondence to: Dr. Bruce L. McNaughton, Department of Neuroscience, Canadian Centre for Behavioural Neuroscience, The University of Lethbridge, 4401 University Dr W, Lethbridge, AB, T1K 3M4, Canada. E-mail: bruce.mcnaughton@uleth.ca and Dr. Corinne J. Montes-Rodriguez, Department of Neuroscience, Canadian Centre for Behavioural Neuroscience, The University of Lethbridge, 4401 University Dr W, Lethbridge, AB, T1K 3M4, Canada. E-mail: corinne.montes@uleth.ca

Qian Lu is currently at University of Calgary, Calgary, AB, T2N 1N4, Canada.

Accepted for publication 21 May 2013.
DOI 10.1002/hipo.22146
Published online 5 July 2013 in Wiley Online Library (wileyonlinelibrary.com).

expression during postnatal development in the rat hippocampus. We hypothesized that the capability to express synaptic plasticity related genes during development might indicate when critical circuit organization processes occur. Hippocampal synaptic plasticity evaluated by the onset of the long term potentiation (LTP) is observed at P5-P7 and the onset of the late phase at P12 (Harris and Teyler, 1984; Bekenstein and Lothman, 1991; Cao and Harris, 2012). To evaluate the maximal capability to express H1a during postnatal development, we used maximal electroconvulsive shock (MECS) treatment as a model of exacerbated synaptic plasticity (Cole et al., 1990) and a home cage (HC) group as a control.

MATERIALS AND METHODS

Subjects, Apparatus, and Behavior

Brown Norway male and female rats at different postnatal (P) ages were used (P3, P5, P7, P9, P11, P15, P19, P23, P35, and adult). Animals were maintained under constant temperature (23°C), humidity (52%), and a controlled 12:12 light-dark cycle (lights on at 07:30 h) with food and water *ad libitum*. On the experimental day, one litter was moved to a different room with the same temperature, humidity and light conditions. All pups from each litter were used on the same day in order to avoid extra stress if any pups remained. Therefore, all the animals experienced the same handling conditions. MECS was induced after attachment of saline-soaked earclips by an electroshock (1.1-s, 100-Hz, 85-mA stimulus of 0.5 ms square-wave pulses) delivered by a constant-current pulse generator (ECT; Ugo Basile, Comerio, Italy) (Cole et al., 1990). The pups were returned to their litter and the brains were removed 25 min after the MECS treatment (Vazdarjanova et al., 2002). Home cage (HC, $N = 2$ per each age point) and MECS ($N = 2$ per each age point) rats were decapitated with a rodent guillotine. All experiments were conducted at the beginning of the dark phase.

Animals were treated in accordance with approved University animal use protocols, the *Guide for the Care and Use of Laboratory Animals* established by the National Institute of Health, and the principles presented in the *Guidelines for the Use of Animals in Neuroscience Research* by the Society for Neuroscience.

Fluorescence *In Situ* Hybridization (FISH)

Brains were hemisected along the midline, quick frozen in isopentane and stored at −80°C for later processing. One hemisphere from each rat at each age point (HC, $N = 2$; and MECS, $N = 2$) was embedded in Tissue-Tek OCT compound. In this manner, all animals at each age point were represented on the same slide. The remaining hemisphere was stored at −80°C for qRT-PCR processing. The Tissue-Tek OCT block was sectioned on a cryostat and 20-μm-thick sagittal sections across the whole brains were obtained. Fluorescence *in situ* hybridization (FISH) for H1a was performed as described previously (Guzowski et al., 1999; Vazdarjanova et al., 2002). H1a antisense riboprobe was generated using an H1a cDNA clone and was directed to the 4.4 kb 3'untranslated region (UTR) of the H1a mRNA (Brakeman et al., 1997; Vazdarjanova et al., 2002). Briefly, riboprobe was synthesized using a commercial transcription kit (MAXIscript Kit; Ambion, Austin, TX) and Fluorescein-labeled UTP (Roche Diagnostics; Indianapolis, IN). It was purified using mini Quick Spin columns (Roche Diagnostics; Indianapolis, IN) and verified by gel electrophoresis. Slides were fixed in 4% paraformaldehyde, incubated in 0.5% acetic anhydride/1.5% triethanolamine, and acetone/methanol (1:1). After washes in SSC, slides were treated with 120 μL of prehybridization buffer (Formamide, 20xSSC, dextran sulfate, DEPC-treated H_2O, Denhardt's solution, Yeast tRNA and salmon sperm DNA) for one hour at room temperature in a humid chamber. H1a riboprobe (1 ng/μL) was diluted in hybridization buffer, heat denatured, chilled on ice, and added to each slide (120 μL). Slides were incubated in a humid chamber at 56 °C for 14 hours. After washes in SSC, slides were washed 30 min in 2xSSC with RNase A (10 μg/mL) at 37°C, treated with 3% H_2O_2 in 1xSSC for 15 min and incubated with TSA-blocking buffer (PerkinElmer, Boston, MA) containing 5% sheep serum for 30 min. Fluorescein-labeled H1a probe was detected with anti-Fluorescein-HRP antibody (1:1000) (Jackson ImmunoResearch Labs, PA) overnight at 4°C and amplified with a Fluorescein-tyramide signal amplification kit (PerkinElmer, Boston, MA). Nuclei were counterstained with 4',6' diamidino-2phenylindole (DAPI; Sigma-Aldrich, St. Louis, MO). Slides were coverslipped with Vectashield (Vector Laboratories, ON, Canada) and sealed with nail polish.

Image Acquisition

Large Scale Imaging

Large scale images of the entire sagittal sections were captured with an automated scanning microscope equipped for wide-field fluorescence (NanoZoomer Digital Pathology RS, Hamamatsu Photonics). A single layer in the middle of the section was scanned at 4x exposure time and 40x resolution with a multi band pass filter cube (DAPI/FITC/Texas Red). Eight sections from $L = 1.6$ to 5.3 were chosen for each age group. Each section corresponded to the same lateral level across ages according to Paxinos and Watson (2007).

Confocal Scanning

Z-stacks of either 0.38 or 0.5 μm optical sections from dorsal subiculum (DS), CA1, CA3, and dentate gyrus (DG) were acquired using a FV1000 laser confocal microscope (Olympus, America Inc.) with either 60X or 40X oil immersion objective lenses ($L = 2.9$ and $L = 3.9$ according to Paxinos and Watson, 2007).

For manual counts, laser sensitivity was set with the P3 group because at this age the intra-nuclear foci (INF) are small

and dim. All the acquisition parameters were kept constant for each brain region within a slide. For the automated analysis of the H1a-INF characteristics, the acquisition parameters were set with the adult group to avoid saturation. All acquisition parameters were kept constant for all slides throughout postnatal development so that we were able to compare the H1a-INF size and intensity throughout all age points.

Image Analysis

Manual Analysis

Manual quantification was performed on confocal stacks of DS, CA1, CA3, and DG by one experimenter who was blind to the age and condition of the sample. Two or three stacks per region were analyzed using ImageJ software (NIH, Bethesda, MD). Only putative neurons were included in the analysis, glial cells were identified by their small and evenly bright nuclei. The total number of neurons was identified based on DAPI staining and H1a positive cells were counted if one or two green dots were colocalized with DAPI. The percentage of H1a positive cells was calculated per stack and averaged per animal for each studied area.

Automated Analysis

Automated analysis was done with NanoZoomer Digital Pathology (NDP) -analysis software and with the IEG-analysis software.

NDP-Analysis Software

The number of H1a-INF in the whole sagittal section was obtained by automated analysis using "NDP-analysis" software (Lu and McNaughton, 2010). Subsequent post-analysis for DS, CA1, CA3, and DG were computed. Briefly, NDP-analysis combined with NanoZoomer Software Development Kit (Hamamatsu NanoZoomer -RS, Olympus) divided the whole image into several sub-images. The automatic FISH signal quantification program was applied to each sub-image separately. The software output includes size, mean intensity, maximum intensity, and location of each H1a-INF detected; the sum of pixels for both the green and the blue channel; and the estimated nuclei number. The information for each automatically segmented INF-FISH signal was stored in both Matlab and Excel formats for future statistical analysis. The segmented FISH signals of each sub-image were superimposed on the original image. And, all the sub-images were stitched back together and saved as a relatively low resolution image for display purposes and image analysis.

NanoZoomer images were preprocessed through several filters to improve the image quality before automated detection of H1a-INF. DAPI bleed-through filter: The blue proportion from the green channel was removed by plotting the green vs. blue pixels intensities. For each level of blue, the minimal green value was extracted. A linear regression was performed between these values and the corresponding value was subtracted from the green channel. Background noise and glial removal: Two binary masks in the blue channel were created. To remove glia cell nuclei, a binary mask in the blue channel with a gray-level value lower than a threshold (in this study, 200 out of 255 set to 1, others set to 0). To remove pixels not detectable by the human eyes in the blue channel (background noise), a mask with gray-level value higher than a threshold (in this study, 25 out of 255 set to 1, others set to 0). These two masks were combined and multiplied by the result of the green channel from the DAPI bleed-through filter. After this, we were able to see the clear FITC spots on the image. Green channel background noise removal: All pixels with an intensity lower than a threshold value (in this study, 15 out of 255) were removed from the green channel image obtained from DAPI bleed-though filter.

FISH spots quantification was performed after the image preprocessing step. A true FISH signal was defined as a group of green pixels (blob) present in the cell nuclei. NDP-analysis identified a FISH blob when it passed the following criteria: (1) The size of a "blob" is > 12 pixels. (2) We measured the mean intensity of the blob in the green channel M(Gj), the mean intensity of the same area of the blob in the blue channel M(Bj), and the sum of intensity of the blob S(Gj). If $M(Gj)-M(Bj) \geq 20$, $S(Gj) \geq 1{,}000$ and $S(Gj) < 10{,}000$, the "blob" was defined as a FISH blob. (3) For blobs with $S(Gj) \geq 10{,}000$ and spot eccentricity larger than 0.80, watershed segmentation was used in order to separate two overlapped spots. Then step 2 was applied again to identify whether each sub-blob generated by watershed algorithm was a real FISH blob or not. Finally, to avoid over-segmentation, if the distance between two neighbouring blobs was less than 25pixels, these two blobs were counted as one FISH blob.

Nuclei Number Estimation

Nuclear diameter was measured manually in the hippocampus and cerebral cortex across all postnatal ages (97 DG nuclei, 69 CA1 nuclei, 34 CA3 nuclei, 58 cerebral cortex layer 2/3 nuclei, and 58 cerebral cortex layer 4/5 nuclei). The average diameter was 12.309 ± 0.089 μm (DG $= 10.790 \pm 0.110$ μm, CA1 $= 12.779 \pm 0.152$ μm, CA3 $= 13.3 \pm 0.320$ μm, cerebral cortex layer $2/3 = 12.831 \pm 0.199$ μm and layer $4/5 = 11.851 \pm 0.114$ μm). The blue channel pixel number was calculated after simple thresholding (15–130). The nuclei number was estimated by the following equations: Nuclei Number = Total Pixel Number/Single Nuclei Area; where Single Nuclei Area $= \pi \times$ (Average Diameter/2/Pixel Size)^2 and Pixel Size = 0.23 μm/ pixel in 40 X magnification NanoZoomer image.

H1a-INF Characteristics with IEG-Analysis Software

In order to calculate reliable INF size and intensity, high resolution confocal z-stacks images were used, which greatly eliminate out-of-focus fluorescence noise (Pawley, 2006). In contrast, this noise is significantly visible in NanoZoomer images in the form of fluorescence rings and blurry INF objects. The images were stored in an uncompressed

multichannel Tiff format to eliminate post acquisition image compression noise.

Images of *z* optical planes were converted into image stacks using ImageJ software (NIH, Bethesda, MD). Image stacks were then processed for automated 3D INF quantification using software plug-ins developed in Java for ImageJ. The software's core algorithm assumes that each INF has a single local maximum represented by a pixel or a group of connected pixels with an intensity (Pi) greater than the user defined threshold value (Ti) and background value (Bi) in 3D space (Du et al., 2011). After discovering the local maxima, the INF object is expanded in 3D space recursively using N-connected pixels. All the connected pixels with an intensity Pi $\geq$ Ti and Pi $\geq$ Bi are included as INF objects. During the final stage, discovered INF objects are validated as per various user defined criteria parameters such as size (SZ), peak deflection (PD), etc. User defined criteria parameters are crucial to filter the noisy INF objects. For example, when the INF object is smaller than the SZ, the final stage validation will remove that particular INF object. Thus, user defined criteria based validation not only filters noisy INF objects but it also provides users some amount of control over the automated INF detection algorithm.

For this study, the following thresholds were used: Minimal Size=10 pix, Minimal Green Intensity=15 for CA1, CA3, DG, and DS. Minimal Blue Intensity=15 for CA1, DG, and DS; Minimal Blue Intensity=10 for CA3. The same parameters were maintained through all ages.

Real Time RT-PCR (qRT-PCR)

The hippocampus was dissected and RNA was extracted with TRIzol reagent (Invitrogen, Carlsbad, CA) according to the manufacturer's instructions. RNA was treated with DNase I (Fermentas Molecular Biology Tools, Burlington, ON) and cleaned with an RNAeasy purification kit (QIAGEN, Crawley, West Sussex).

cDNA Synthesis

cDNA was made using iScriptSelect cDNA Synthesis Kit (Bio-Rad Laboratories, Mississauga, ON, Canada) according to the manufacturer's instructions. Briefly, 500 ng of RNA were reverse-transcribed with 2 μL of iScript reverse transcriptase, RNase inhibitor protein, and oligo $(dT)_{20}$, in a total volume of 20 μL. Reaction was carried out at 42°C for 60 min. Reverse transcriptase was heat-inactivated at 85°C for 5 min.

qRT-PCR

Primers for H1a and ß-Actin were designed using PrimerQuest software (Integrated DNA Technologies, Inc) based on the rat sequences deposited in GenBank at the National Center for Biotechnology Information. The primer sequences for H1a were: forward, TACAGCGATTGCAGGAGACATGGT; reverse, ACACTGCAGGGAACTTTACGGTCT. The primers for ß-Actin were: forward, TCTCTTCCAGCCTTCCTT; reverse, ATGTCAACGTCACACTTCA. qRT-PCR was done using SsoFast EvaGreen Supermix (Bio-Rad Laboratories Ltd., Mississauga, ON) and CFX96 system (Bio-Rad Laboratories Ltd., Mississauga, ON, Canada) according to the manufacturer's instructions. Briefly, 10 μl of 2× SsoFast EvaGreen Supermix, 0.5 μl of 10 mM corresponding forward and reverse primer, and 1 μl of each cDNA sample was prepared in a total volume of 20 μl. qRT-PCR cycling conditions were as follows: enzyme activation 95°C for 30 s, denaturation 95°C for 5 s, annealing/extension 51°C for 5 s (45 cycles), melting curve 65–95°C (5 s/step). Samples were ran in triplicate. A melt curve analysis was conducted, and the specificity of the amplified products was confirmed by a single peak on the melt curve. The Ct values were calculated with CFX Manager 2.0 software. All mRNA expression levels were normalized to the β-Actin mRNA expression.

Statistical Analysis

Statistical analysis was performed using SigmaStat Version 3.5 (Systat Software, Inc.). Two-Way ANOVA tests or Kruskal-Wallis One Way ANOVA on ranks tests followed by the appropriate post-hoc tests were used in Figures 1, 2, 4 (age*treatment), and 5 (age*bin). One-Way ANOVA tests or Mann-Whitney Rank Sum tests were used in Figure 6. Differences were considered statistically significant if the *P*-value was ≤ 0.05.

RESULTS

Automated Analysis of Complete Sagittal Sections Reveals That MECS-Induced H1a Expression Peaks During the Third Postnatal Week

NDP-analysis software detected H1a-INF successfully after the second postnatal week (Fig. 1D). During the first postnatal week, most of H1a-INF did not pass the size and intensity thresholds required for the automated detection. This is reflected in the estimated mean intensity which increases gradually throughout postnatal development in the MECS group ($P < 0.001$; Fig. 1A) (P3-7, 49.386 ± 1.846; P9-15, 63.826 ± 3.093; P19-23, 76.159 ± 1.692; P35-Ad, 70.977 ± 0.712).

MECS-induced H1a expression was observed after the second postnatal week (Figs. 1A–C). An increase in H1a expression was observed in the mean intensity ($P < 0.001$), the percentage of H1a-positive cells ($P < 0.001$), and the intensity ratio ($P < 0.005$). Moreover, the percentage of H1a positive cells peaked during the third postnatal week ($P < 0.003$; Fig. 1B); (P3-7, 1.712 ± 1.007; P9-15, 15.477 ± 2.480; P19-23, 25.070 ± 3.055; P35-Ad, 17.178 ± 0.902). As expected, in the HC group the percentage of H1a-positive cells and the intensity ratio did not change during postnatal development ($P > 0.05$) (Figs. 1B,C).

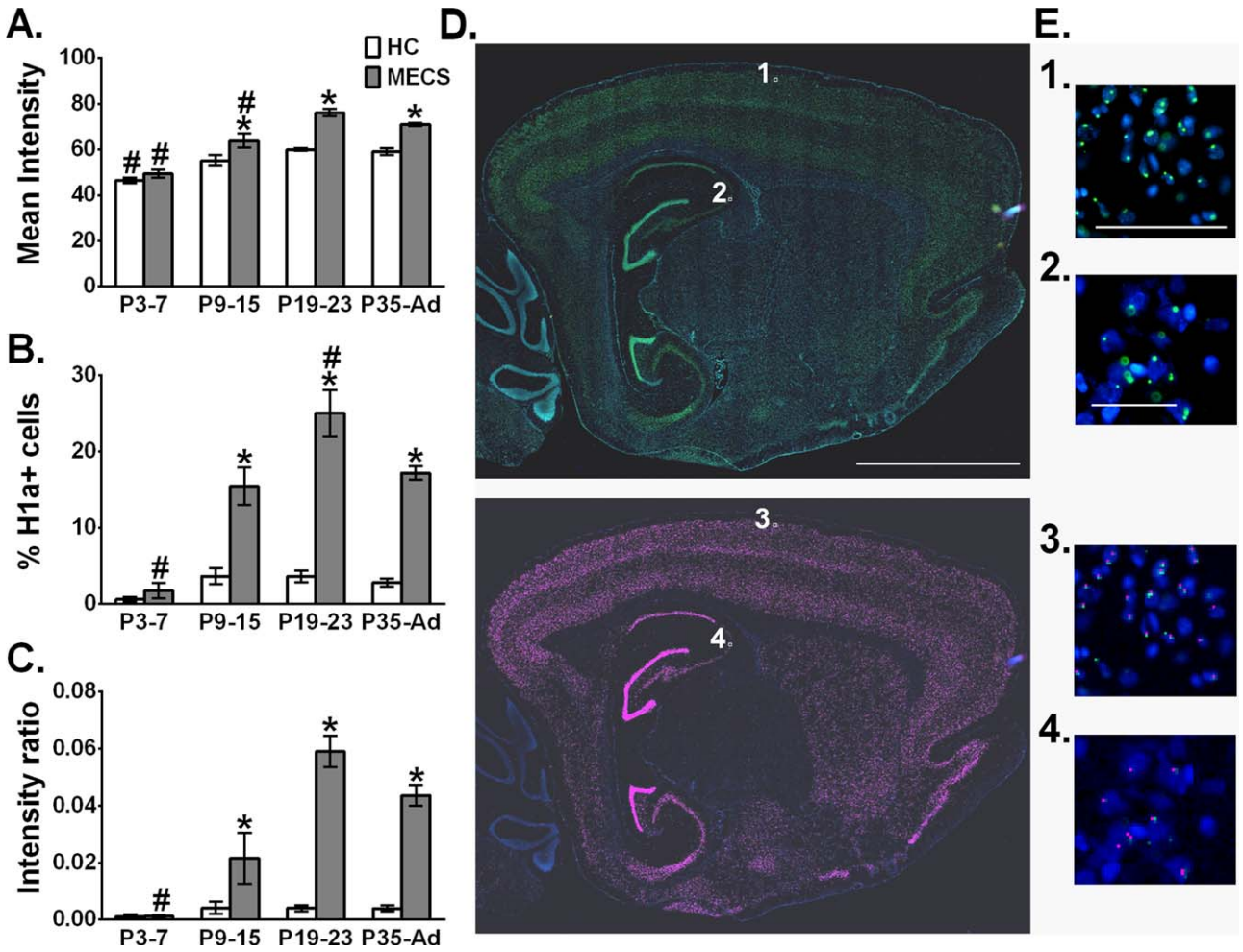

FIGURE 1. Automated analysis of H1a expression during postnatal development in entire sagittal sections. MECS-induced H1a expression appears in the second postnatal week (A–C). A: Mean intensity of detected H1a-INF increases in the second week of life in both Home Cage and MECS groups. MECS increases the mean intensity of the H1a-INF in the second postnatal week. B: The percentage of H1a positive cells induced by MECS changes across postnatal development. Notice that there are no differences between Home Cage and MECS groups during the first postnatal week. C: Intensity ratio was calculated as Sum of the Pixel Intensity in the Green Channel/Sum of the Pixel Intensity in the Blue Channel of the whole image (H1a/DAPI). D: Representative sagittal section of a P35 animal after MECS, acquired with NanoZoomer microscope. The green signal corresponds to H1a-INF (upper panel). The same sagittal section processed with NDP-analysis software. Each H1a-INF was marked by a pink dot (lower panel). Scale bar, 4 mm. E. Insets of the cerebral cortex (1, 3) and CA3 (2, 4). Scale bar 100 µm and 50 µm respectively. *$P \leq 0.05$, Home Cage different from MECS. #$P \leq 0.05$, different from all the other age groups under the same condition. Data are presented as Mean ± S.E.M. Groups: P3-7 ($N = 6$); P9-15 ($N = 6$); P19-23 ($N = 4$); P35-Ad ($N = 4$) in both HC and MECS groups. [Color figure can be viewed in the online issue, which is available at wileyonlinelibrary.com.]

Hippocampal Regional Analysis Indicates That the Number of H1a Positive Cells Reaches Adult Levels at P9

Regional analysis in the hippocampus was made on both confocal and NanoZoomer images. Manual quantification revealed that H1a expression is present at P3 in a significant proportion of cells (around 40%) in DS, CA1, and CA3, (Figs. 2A,C,E and 3). However, H1a-INF are small and dim (Figs. 3 and 4D). Both MECS and HC groups exhibit the same amount of H1a positive cells during the first postnatal week (DS, $P = 0.332$; CA1, $P = 0.501$; CA3, $P = 0.553$; DG, $P = 0.114$) (Fig. 2). Automated quantification on NanoZoomer images showed similar results (Figs. 2B,D,F,H). This confirms that MECS was not able to induce H1a expression at this age.

MECS-induced H1a expression in the hippocampus was observed after the second postnatal week (Fig. 2). Both, manual (Figs. 2A,C,E,G) and automated (Figs. 2B,D,F,H) quantification showed the same effect.

MECS-induced H1a positive cells reached a plateau in the second week of life for DS and CA3 (Figs. 2A, E, and 3). However, a gradual increase in the number of H1a-positive cells was observed in the DG with both manual ($P < 0.001$

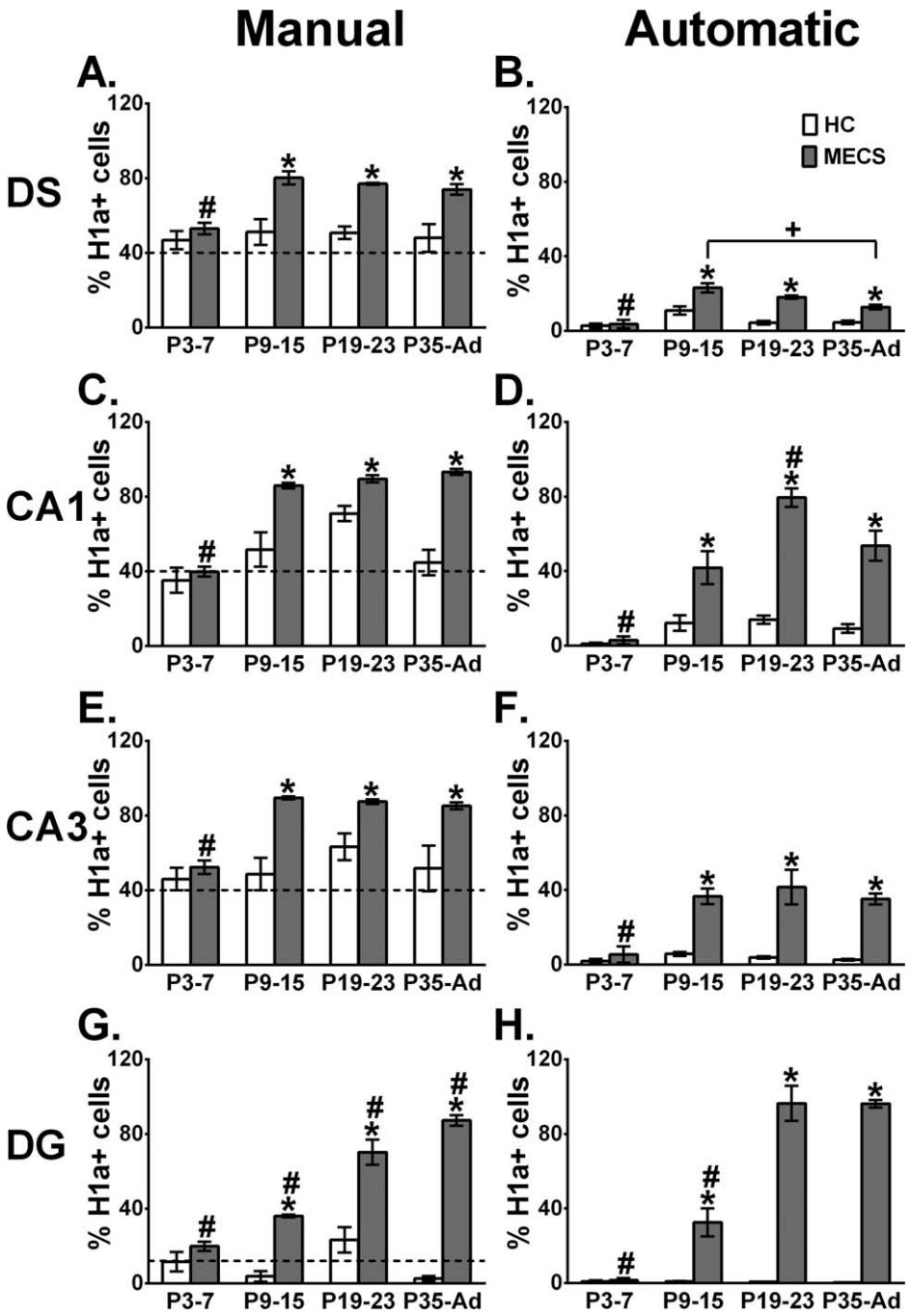

FIGURE 2. Regional analysis of H1a postnatal development in the rat hippocampus. Manual counts on confocal stacks (A, C, E, G) and automatic counts on NanoZoomer images (B, D, F, H) are shown. MECS-induced H1a expression occurs in the second postnatal week for all analyzed regions: dorsal subiculum (DS) (A, B); CA1 (C, D); CA3 (E, F) and dentate gyrus (DG) (G, H). A high proportion of H1a positive cells (around 40%) was observed since the first postnatal week on the confocal images (A, C, E). However, in the automatic analysis (B, D, F, H) most of the H1a-INF were not detected since the software detects only INF above threshold intensity and size. The number of H1a-positive cells reaches adult levels in the second postnatal week in DS (A, B), CA1 (C, D) and CA3 (E, F). DG exhibits a linear increase across postnatal development; in the adult, H1a expression is induced by MECS in more than 95% of granule cells (G, H). If a post-hoc threshold is applied to the manual quantification plots (dashed lines), manual and automatic analyses appear more similar. Peaks of H1a expression were detected by automatic analysis in CA1 and DS. * $p \leq 0.05$, Home Cage different from MECS. #$P \leq 0.05$, different from all the other age groups under the same condition. Data are presented as Mean ± S.E.M. "P" value from manual counts as follows: In DS, P9-15, $P < 0.001$; P19-23, $P = 0.002$; and P35-Ad, $P = 0.002$. In CA1, P9-15, $P < 0.001$; P19-23, $P = 0.035$; and P35-Ad, $P = 0.001$. In CA3, P9-15, $P < 0.001$; P19-23, $P = 0.019$; P35-Ad, $P = 0.002$. In DG, P9-15, P19-23 and P35-Ad, $P < 0.001$. The same trend was observed in the automated quantification: in DS, P9-P15 and P19-23, $P < 0.001$; P35-Ad, $P = 0.011$; CA1, $P < 0.001$ for all groups; CA3, $P < 0.001$ for all groups; and DG $P < 0.001$ for all groups. Groups: P3-7 (N=6); P9-15 (N=6); P19-23 (N=4); P35-Ad ($N = 4$).

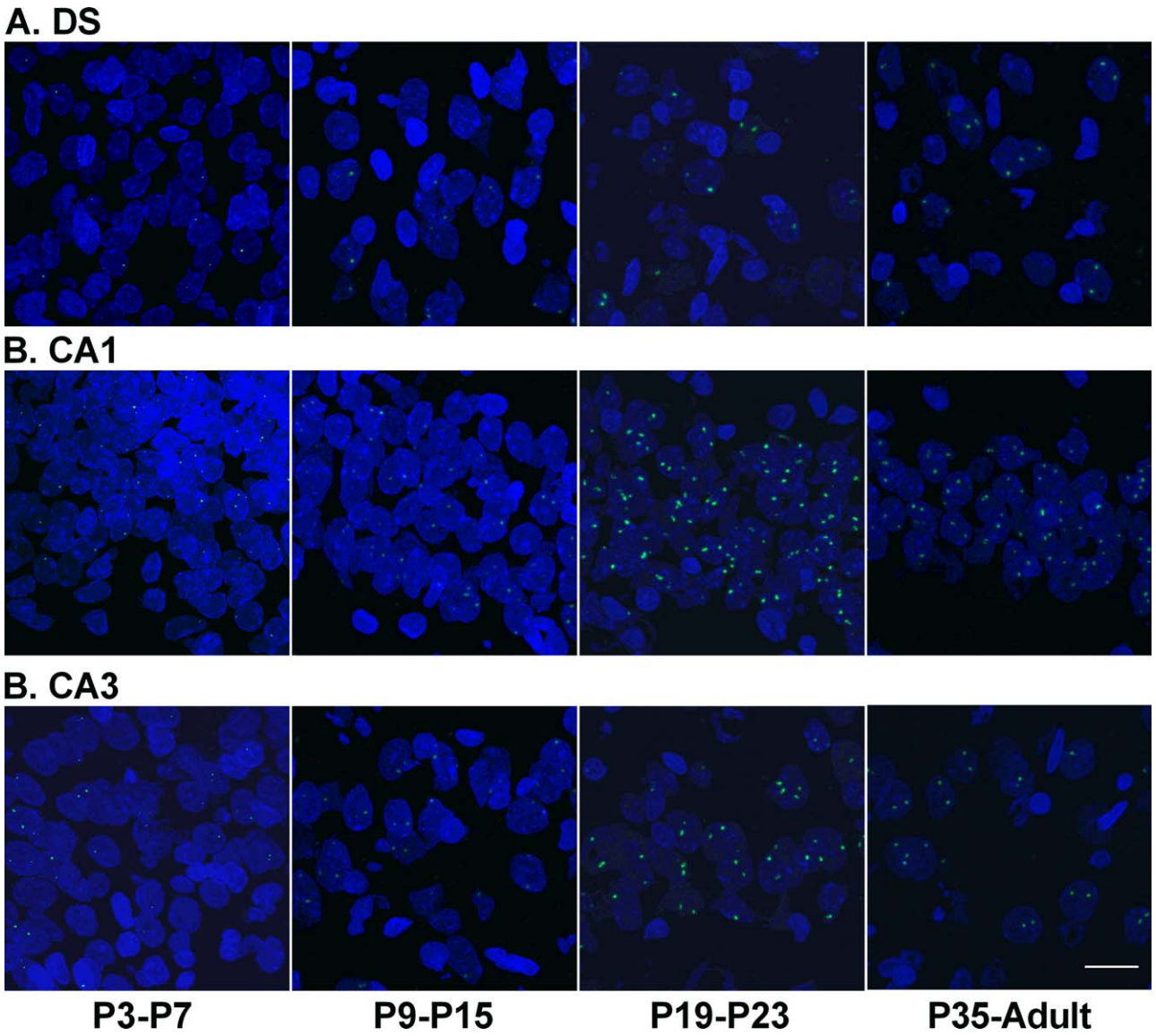

FIGURE 3. MECS-induced H1a expression across postnatal development. A–C: Maximal intensity projections of confocal *z*-stacks of dorsal subiculum (DS) (A.), CA1 (B.) and CA3 (C.) after MECS at 60x magnification. Green dots are H1a-INF and nuclei were counterstained with DAPI. Notice that H1a-INF are small and less intense during the first two postnatal weeks compared with adults; this is more obvious in CA1 (B.) and CA3 (C.). Scale bar, 20 µm. The number of MECS-induced H1a positive cells does not change after P9 but the H1a-INF characteristics are different. [Color figure can be viewed in the online issue, which is available at wileyonlinelibrary.com.]

for all groups; Fig. 2G) and automated ($P < 0.001$ for P3-7 and P9-15 compare to all ages; Fig. 2H) quantification.

No differences were observed in the HC group during postnatal development in all analyzed regions ($P > 0.05$), for both manual and automated quantification. The DG showed almost no H1a expression in the HC group (Figs. 2G,H).

In addition, automated quantification showed that MECS-induced H1a expression peaks in DS (Fig. 2B) and CA1 (Fig. 2D). In DS, the P9-15 is different from P3-7 and P35-Ad groups ($P < 0.001$), while in CA1, the P19-23 group is statistically different from all ages ($P < 0.001$). Given that we did not observe the same peaks in the manual analysis and because the automated quantification computed the number of INF based on size and intensity parameters, we decided to analyze the size and intensity of H1a-INF which clearly changed across postnatal ages (Fig. 3).

H1a-INF Size and Intensity Change Across Postnatal Development

A detailed analysis of H1a-INF size and intensity in confocal stacks indicated that hippocampal H1a-INF change across postnatal development in the MECS condition (Fig. 4). The HC group did not exhibit any significant change (Fig. 4).

In DS, the average and maximum intensity of H1a-INF increased at P9-15 and P19-23 (Fig. 4A). The mean intensity

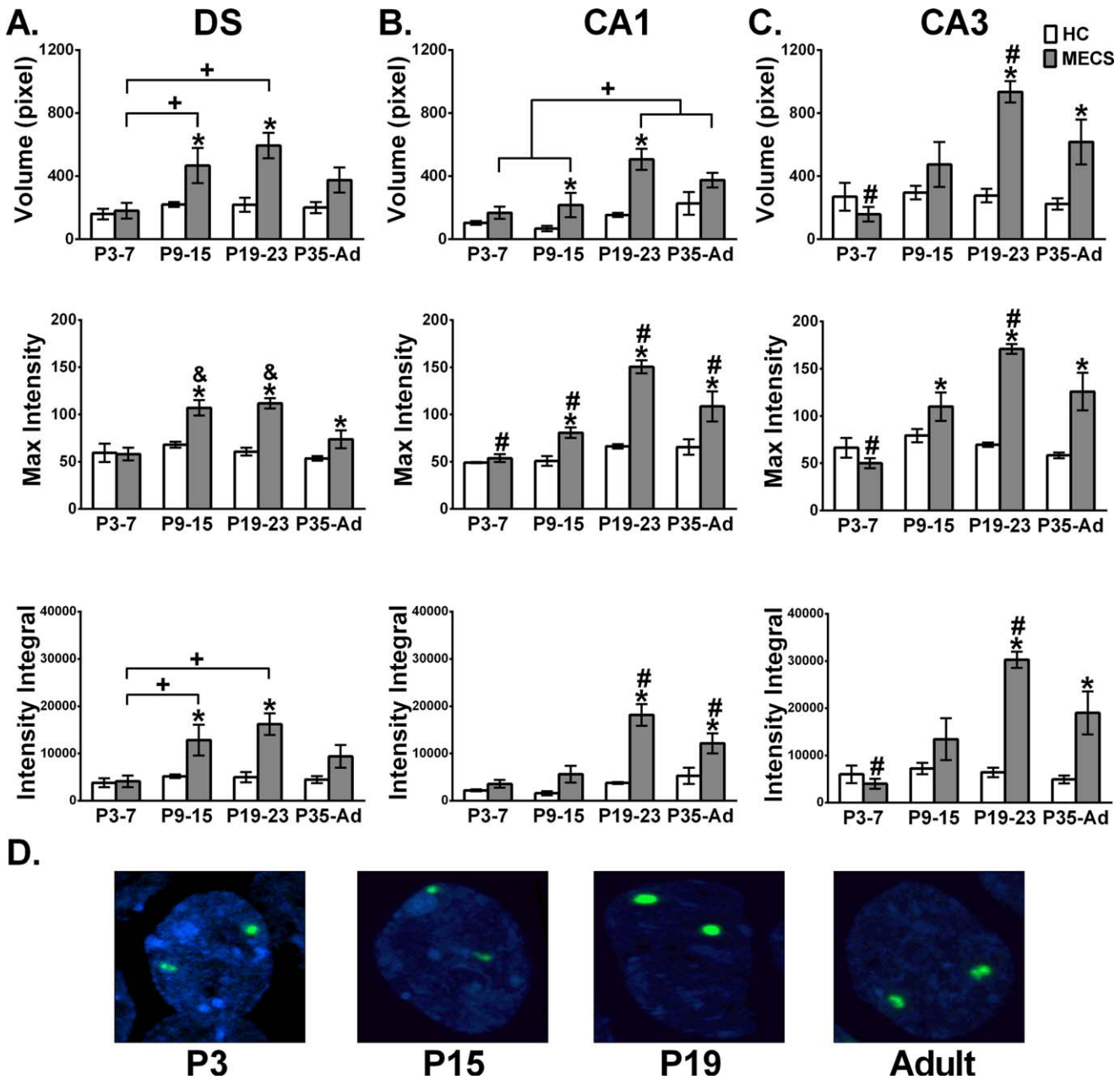

FIGURE 4. The H1a-INF volume and intensity increase across postnatal development and peak at P9-23. A: In dorsal subiculum (DS), H1a-INF volume and intensity peak during the second and third postnatal week in the MECS group. B: H1a-INF volume and intensity increase across postnatal development in CA1 and peak at P19-P23 in the MECS group. C: In CA3, the volume, maximal intensity and intensity integral of H1a-INF peak at P19-P23 in the MECS group. *$P \leq 0.05$, Home Cage different from MECS. #$P \leq 0.05$, different from all the other age groups under the same condition. &$P \leq 0.05$, different fromP3-7 and P35-Ad. +$P \leq 0.05$, lines indicate statistical differences. Data is presented as Mean ± S.E.M. Groups: P3-7 (N = 3-4); P9-15 (N = 4); P19-23 (N = 4); P35-Ad (N = 3). [Color figure can be viewed in the online issue, which is available at wileyonlinelibrary.com.]

at P9-15 is different from P3-7 and P35-Ad ($P < 0.001$ and $P = 0.006$ respectively); and at P19-23 is different from P3-7 and P35-Ad ($P < 0.001$ and $P = 0.003$ respectively). The maximum intensity at P9-15 and P19-23 is different from P3-7 ($P \leq 0.002$) and from P35-Ad ($P \leq 0.004$). The volume and intensity integral increased at P19-23 (Fig. 4A). The volume at P19-23 is different from P3-7 and P35-Ad ($P = 0.01$ and $P = 0.002$ respectively); and the intensity integral at P19-23 is different from P3-7 ($P = 0.004$) and from P35-Ad ($P = 0.005$).

In CA1, H1a-INF size and intensity increased at P19-23 (Fig. 4B). This was observed in the mean intensity (P19-23 vs. P3-7 and P9-15, $P < 0.001$; P19-23 vs. P35-Ad, $P = 0.012$), the maximal intensity (P19-23 vs. all groups, $P < 0.001$) and

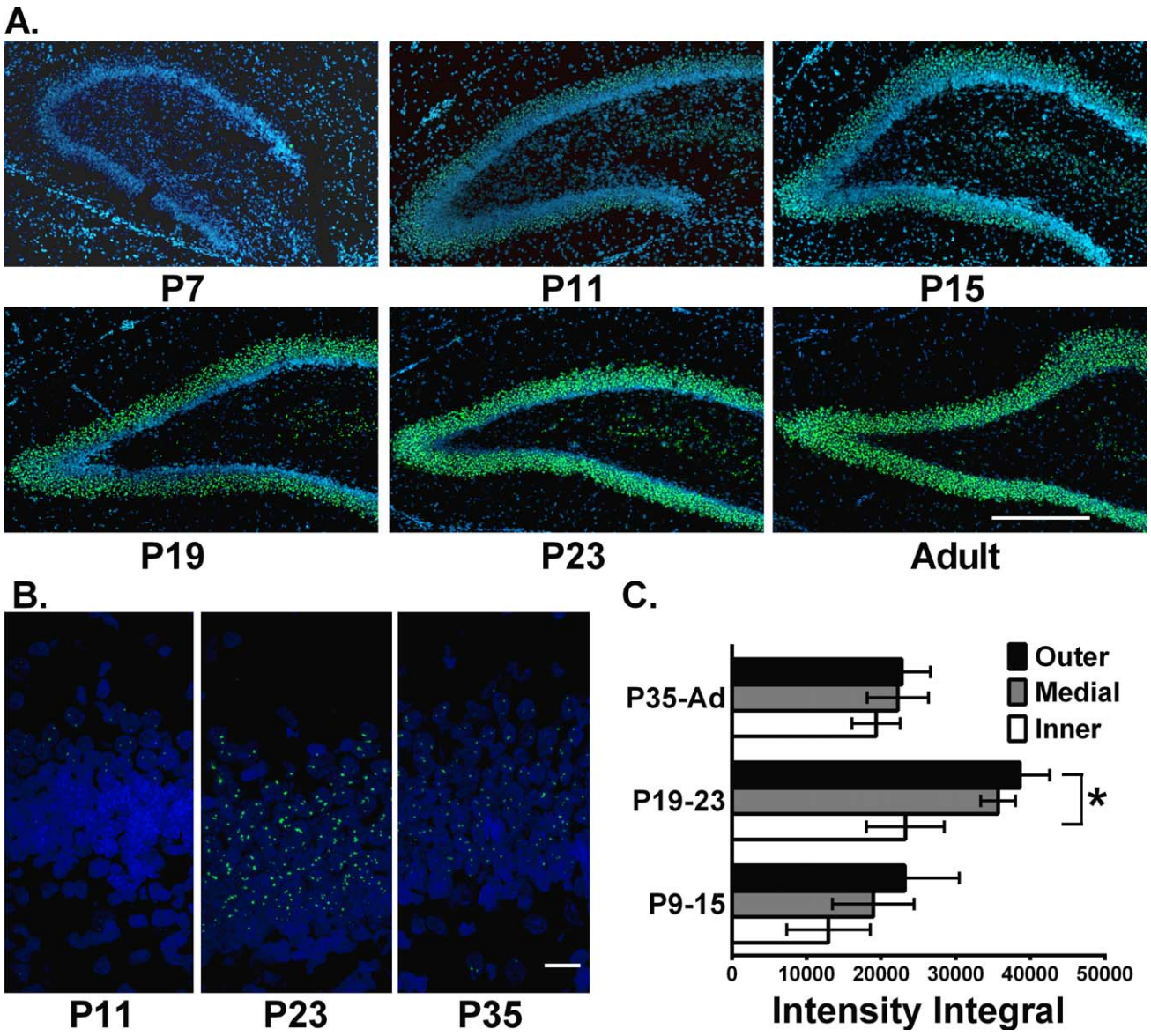

FIGURE 5. Lamination pattern of H1a expression in the dentate gyrus (DG) during postnatal development mirrors the normal maturation of granule cells. A: Images acquired with NanoZoomer microscope. H1a positive cells appear in the outer portion of the granule cell layer and become thicker up to about P35. Scale bar, 500 μm. B: Maximal intensity projections of confocal *z*-stacks of DG at 60X. An H1a-INF gradient is observed in the granule cell layer. H1a-INF in the outer portion are bigger and brighter than in the inner portion of granule cells. Scale bar, 20 μm. C. The biggest and brightest H1a-INF are observed in mature neurons. The granule cell layer was divided in three bins and a mean of the H1a-INF integral intensity per bin was calculated. *$P \leq 0.05$. Two way-ANOVA test was used (age * bin). Data are presented as Mean ± S.E.M. Groups: P9-15 ($N = 3$); P19-23 ($N = 3$); P35-Ad ($N = 3$). [Color figure can be viewed in the online issue, which is available at wileyonlinelibrary.com.]

the intensity integral (P19-23 *vs* P3-7 and P9-15, $P < 0.001$; P19-23 vs. P35-Ad, $P = 0.01$).

A similar trend was observed in CA3 (Fig. 4C); H1a-INF size and intensity increase at P19-23. This was reflected in the volume (P19-23 vs. P3-7, $P < 0.001$; P19-23 vs. P9-15, $P = 0.002$; P19-23 vs. P35-Ad, $P = 0.017$), maximum intensity (P19-23 vs. P3-7 and P9-15, $P < 0.001$; P19-23 vs. P35-Ad, $P = 0.004$) and intensity integral (P19-23 vs. P3-7 and P9-15, $P < 0.001$; P19-23 vs. P35-Ad, $P = 0.006$).

Laminar Maturation of H1a in the DG During Postnatal Development

A laminar maturation of the DG was observed; H1a positive cells induced by MECS appeared in the outer portion of the granule cell layer at the beginning of postnatal development, with the boundary moving towards the inner portion later on (Fig. 5A). At P35 H1a is not yet expressed in all granule cells but is expressed in more than 95% in the adult (Figs. 2G,H).

Moreover, H1a expression appeared first in the suprapyramidal layer and later on in the infrapyramidal layer, following the normal granule cells maturation.

Interestingly, a gradient in the H1a-INF size and intensity was observed across the granule cell layer of DG. The brightest and biggest INF were observed in the outer portion which mainly contains mature neurons, whereas the smallest INF were observed in the internal portion of the DG which contains mainly immature neurons (Figs. 5A–C). The difference between the inner and the outer portion of the granule layer was striking at P19-23 ($P = 0.035$, Fig. 5C). Moreover, the H1a-INF size and intensity gradient was more evident earlier in development, when more immature neurons are present, than in the adult (Fig. 5C).

H1a mRNA and INF Volume and Intensity Increase Across Postnatal Development in the Hippocampus

Since H1a-INF size and intensity might reflect the amount of H1a mRNA, we performed qRT-PCR for H1a in the hippocampus of MECS animals. H1a mRNA increased progressively during postnatal development (Fig. 6C); $P \leq 0.001$, P3 compared with P19-23 and P35-Ad; $P \leq 0.02$, P9-15 compared with P19-23 and P35-Ad.

To compare the H1a-INF characteristics with H1a mRNA obtained from the whole hippocampus, the intensity integral of all analyzed stacks from DS, CA1, CA3, and DG were averaged. The intensity integral increased throughout postnatal development (Fig. 6A). In addition, the total green intensity/total blue intensity (intensity ratio) from each confocal stack was obtained and averaged. The intensity ratio also increased throughout postnatal development (Fig. 6B).

Our results indicate that the H1a mRNA levels induced by MECS increased across postnatal development and this was reflected in the H1a-INF characteristics and intensity ratio.

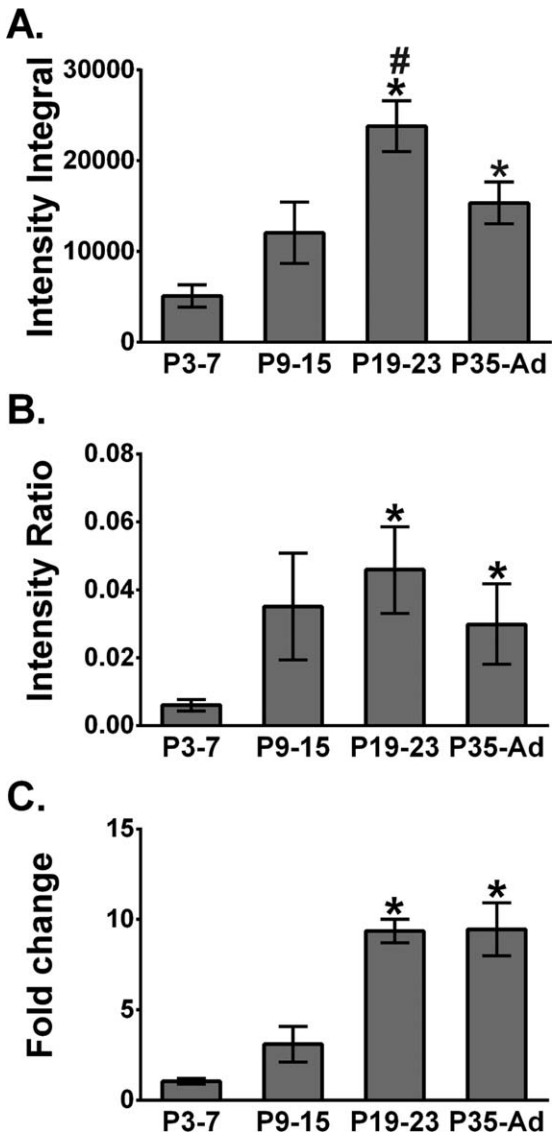

FIGURE 6. H1a-INF volume and intensity are indicators of H1a mRNA levels in the MECS group. A: H1a-INF intensity integral in the hippocampal systems increases during postnatal development in the MECS group. B: Intensity ratio was calculated by dividing the Sum of the Pixel Intensity in the Green Channel by the Sum of the Pixel Intensity in the Blue Channel of confocal stacks from all the hippocampal regions. The intensity ratio increases throughout postnatal development. C: qRT-PCR indicates that H1a H1ahmRNA levels increase during postnatal development in the hippocampus. *$P \leq 0.05$, different from P3-7 group. #$P \leq 0.05$, different from all the other groups. Groups: H1a-INF and Intensity Ratio P3-7 ($N = 3$-4); P9-15 ($N = 4$); P19-23 ($N = 4$); P35-Ad ($N = 3$-4). qRT-PCR P3-7 ($N = 5$); P9-15 ($N = 5$); P19-23 ($N = 6$); P35-Ad ($N = 6$).

DISCUSSION

The assembly and refinement of neural circuits are critically regulated by neuronal activity and related synaptic mechanisms (O'Donovan, 1999; Kirov et al., 2004; Maffei and Turrigano et al., 2008; De Roo et al., 2008). IEGs convert neuronal activity into stable synaptic connections (Kubik et al., 2007) indicating an important role for these genes during the formation of neural circuits. Brakeman et al., 1997 showed that H1a is spontaneously up-regulated in rat forebrain around the third postnatal week, suggesting that H1a-dependent synaptic plasticity could be also developmentally regulated. In this study, we used MECS as a means of maximizing H1a expression.

Our results indicate that, a large population of cells (40%) in both MECS and HC groups were H1a positive at P3 in the DS, CA1, and CA3 (Figs. 2A,C,E). In the HC group, this proportion did not change across postnatal development (Figs. 1B and 2) as previously reported by Kato et al., 1998. The percentage of H1a positive cells in our control group is higher than previous studies (Vazdarjanova et al., 2002, 2004; Bottai et al., 2002). This could be caused by diurnal variations in home cage behavior; our animals were killed at the beginning of the dark phase when there was likely an increase in general

arousal and motor activity. Increases in H1a expression in dark phase have been reported by others (Maret et al., 2007).

Interestingly, although all the animals exhibited a clear behavioral response to the electroshock (i.e. seizures, spasticity), MECS did not increase H1a expression until the second postnatal week in all analyzed regions (Figs. 1A–C and 2). This indicates the absence of activity dependent-synaptic plasticity related to H1a expression during the first postnatal week. Previous studies have also shown the absence of *c-fos* induction after seizures at P4 and P7 in rats (Schreiber et al., 1992), and in immature mice (Storey et al., 2002). In both cases, the mRNA is present in the immature brain but it is not up-regulated after seizures as in the mature brain.

The fact that H1a-dependent plasticity appears at the same time in all regions suggests a general maturation process corresponding with the beginning of the glutamatergic transmission maturation (Durand et al., 1996; Ben Ari et al., 1997; Garaschuck et al., 1998) and the switch of GABA actions from excitatory to inhibitory (Ben Ari et al., 1997; Tizio et al., 2007). It is possible that H1a cannot be up-regulated during the first postnatal week because glutamatergic transmission is immature, supporting the interrelation between glutamatergic actions and H1a-dependent synaptic plasticity (Brakeman et al., 1997; Kato et al, 1998; Ango et al., 2000; Lominac et al., 2005; Inoue et al., 2007). In immature neurons, on the other hand, the electrochemical equilibrium potential for Cl^- is more depolarized than the resting potential, indicating an elevated intracellular concentration of Cl^- that promotes GABA excitatory activity (Ben Ari et al., 2002). In fact, it has been shown that the increased seizure susceptibility during early postnatal development is due to the depolarizing actions of GABA (Khazipov et al., 2004). Therefore, it is also possible that the seizures observed after MECS were due to GABA depolarizing actions. Altogether, this may affect the dynamics of neuronal depolarization in immature synapses and suggests that H1a was not up-regulated during the first postnatal week because depolarization level may be reduced in neonates (Durand et al., 1996; Ben-Ari, 2002). However, the specific cellular mechanism that underlies the absence of MECS-induced H1a needs to be addressed. For example, it is also possible that cellular signalling mechanisms underlying electro-transcriptional coupling for H1a may be immature.

In the DG, MECS-induced H1a expression exhibited a laminar pattern (Fig. 5) that parallels the normal granule cells maturation (Ye et al., 2000; Rahimi and Claiborne, 2007). The first MECS-induced H1a positive cells were observed at the end of the first postnatal week, which correlates with the first adult-like cells at P7 (Jones et al., 2003). H1a positive cells were observed in the outer portion of the granule layer that corresponds to mature neurons, the "H1a layer" thickness increased gradually throughout postnatal development until the adult stage (Fig. 5). A similar laminar pattern has been shown for *fos-lacZ* expression where the totality of the granule cell layer expresses this gene by P20 (Vendrell et al., 1998); and for *Arc* expression where the laminar pattern was followed until P15 (McNaughton et al., 2007). Likewise, the INF size and intensity gradient indicates that the mature neurons exhibit the biggest and brightest foci (Figs. 6B,C). Moreover, the cell position within the granule cell layer correlates with glutamatergic maturation and synaptic efficiency (Ye et al., 2000; Jones et al., 2003; Ambrogini et al., 2004), further supporting the relationship between H1a expression and synaptic maturation.

H1a-INF size and intensity in the MECS group increased at P19-23 (Fig. 4). At this age, glutamatergic and GABAergic transmissions are mature (Rao et al., 1998; Shiraishi et al., 2003; Anderson et al., 2004; Tizio et al., 2007) and a rudimentary spatial system is already present (head directional cells emerge at P15-16, place cells at P16-18 and grid cells at P19-20) (Langston et al., 2010; Wills et al., 2010). Similarly, the increase of H1a expression in the parasagittal sections is observed after the synaptogenesis period in the hippocampus from P4 to P14 (Biranowska et al., 2002) and in the neocortex from P11 to P20 (Sutor and Luhmann, 1995). At the end of the third postnatal week, hippocampal synapses are functionally mature and this correlates with the observed peak of H1a expression (P19-23 group). Synapse stabilization requires specific gene expression, regulation of mRNA translation, and de novo proteins synthesis (Yoshihara et al., 2009). Suggesting that the observed H1a peaks of expression could be related to activity dependent refinement of neuronal circuits during postnatal development. This idea is further supported by the role of H1a in LTD (Hu et al., 2010), the relationship between LTD and synapse elimination (Bastrikova et al., 2008) and the developmental switch at P21 of LTD mediated by postsynaptic mechanisms and protein synthesis (Nosyreva and Huber, 2005). In addition, H1a negatively regulates synaptic growth in hippocampal neurons (Sala et al., 2003) and is positively involved in activity-induced synaptic remodeling (Inoue et al., 2007), indicating its critical role in synaptic rearrangement.

We also provide evidence that the INF size and intensity evaluated by FISH reflects the amount of mRNA present (Fig. 6). This relationship became clear after we normalized the FISH signal of positive cells (Fig. 6A) against the blue pixel intensity (DAPI) that represents the number of cells (Fig. 6B). In this way, we compare the normalized H1a signal (Fig. 6B) to the qPCR data which includes all cells in the hippocampus (Fig. 6C). Previous works have reported INF intensity changes associated with behavioural and aging conditions (Miyashita et al., 2009; Penner et al., 2011; Witharana et al., 2011). The use of INF-size and intensity as indicators of the amount of mRNA produced by a single neuron may be considered a new element of the cellular compartment analysis of temporal activity by FISH (catFISH) method (Guzowski et al., 2005).

In summary, during the first postnatal week H1a up-regulation is not activity dependent, and, although the maximum number of cells capable of expressing H1a after MECS reaches adult levels at P9, the H1a-INF size and intensity peak at P19-23. The H1a-INF peak parallels synaptic maturation, supporting a functional role for H1a during postnatal neuronal assembly and disassembly. Moreover, the role of H1a as a mediator of synaptic refinement may further explain the H1a activity dependent plasticity processes observed in adult. This

conclusion is supported by recent work showing that H1a induced by an epileptiform stimulus promotes synapse loss in hippocampal cultures (Li et al., 2013)

Acknowledgements

The authors thank Dr. A. Golubov and A. Babenko for their assistance with qRT-PCR, D. Bray for technical assistance, A. Gomez-Palacio-Schjetnan for discussion and comments and A. Mauthe-Kaddoura for proofreading.

REFERENCES

Ambrogini P, Lattanzi D, Ciuffoli S, Agostini D, Bertini L, Stocchi V, Santi S, Cuppini R. 2004. Morpho-functional characterization of neuronal cells at different stages of maturation in granule cell layer of adult rat dentate gyrus. Brain Res 1017:21–31.

Anderson TR, Shah PA, Benson DL. 2004. Maturation of glutamatergic and GABAergic synapse composition in hippocampal neurons. Neuropharmacology 47:694–705.

Ango F, Pin JP, Tu JC, Xiao B, Worley PF, Bockaert J, Fagni L. 2000. Dendritic and axonal targeting of type 5 metabotropic glutamate receptor is regulated by homer1 proteins and neuronal excitation. J Neurosci 20:8710–8716.

Ango F, Prézeau L, Muller T, Tu JC, Xiao B, Worley PF, Pin JP, Bockaert J, Fagni L. 2001. Agonist-independent activation of metabotropic glutamate receptors by the intracellular protein Homer. Nature 411:962–965.

Bastrikova N, Gardner GA, Reece JM, Jeromin A, Dudek SM. 2008. Synapse elimination accompanies functional plasticity in hippocampal neurons. Proc Natl Acad Sci USA 105:3123–3127.

Bekenstein JW, Lothman EW. 1991. An in vivo study of the ontogeny of long-term potentiation (LTP) in the CA1 region and in the dentate gyrus of the rat hippocampal formation. Brain Res Dev Brain Res 63:245–251.

Ben-Ari Y. 2002. Excitatory actions of gaba during development: the nature of the nurture. Nat Rev Neurosci 3:728–739.

Ben-Ari Y, Khazipov R, Leinekugel X, Caillard O, Gaiarsa JL. 1997. GABAA, NMDA and AMPA receptors: A developmentally regulated 'ménage à trois'. Trends Neurosci 20:523–529.

Biranowska J, Dziewiatkowski J, Ludkiewicz B, Moryś J. 2002. Developmental changes of synaptic proteins expression within the hippocampal formation of the rat. Anat Embryol (Berl) 206:85–96.

Blankenship AG, Feller MB. 2009. Mechanisms underlying spontaneous patterned activity in developing neural circuits. Nat Rev Neurosci 11:18–29.

Bottai D, Guzowski JF, Schwarz MK, Kang SH, Xiao B, Lanahan A, Worley PF, Seeburg PH. 2002. Synaptic activity-induced conversion of intronic to exonic sequence in Homer 1 immediate early gene expression. J Neurosci 22:167–175.

Brakeman PR, Lanahan AA, O'Brien R, Roche K, Barnes CA, Huganir RL, Worley PF. 1997. Homer: a protein that selectively binds metabotropic glutamate receptors. Nature 386:284–288.

Buhl DL, Buzsáki G. 2005. Developmental emergence of hippocampal fast-field "ripple" oscillations in the behaving rat pups. Neuroscience 134:1423–1430.

Cao G, Harris KM. 2012. Developmental regulation of the late phase of long-term potentiation (L-LTP) and metaplasticity in hippocampal area CA1 of the rat. J Neurophysiol 107:902–912.

Cole AJ, Abu-Shakra S, Saffen DW, Baraban JM, Worley PF. 1990. Rapid rise in transcription factor mRNAs in rat brain after electroshock-induced seizures. J Neurochem 55:1920–1927.

De Roo M, Klauser P, Mendez P, Poglia L, Muller D. 2008 Activity-dependent PSD formation and stabilization of newly formed spines in hippocampal slice cultures. Cereb Cortex 18:151–161.

Du G, Drexler GA, Friedland W, Greubel C, Hable V, Kugler A, Krücken R, Tonelli L, Friedl A and Dollinger G. 2011. Spatial dynamics of DNA damage response protein foci along the ion trajectory of high-LET particles. Radiat Res 176:706–715.

Durand GM, Kovalchuk Y, Konnerth A. 1996. Long-term potentiation and functional synapse induction in developing hippocampus. Nature 381:71–75.

Flavell SW, Greenberg ME. 2008. Signalling mechanisms linking neuronal activity to gene expression and plasticity of nervous system. Annu Rev Neurosci 31:563–590.

Foa L, Rajan I, Haas K, Wu GY, Brakeman P, Worley P, Cline H. 2001. The scaffold protein, Homer 1b/c, regulates axon pathfinding in the central nervous system in vivo. Nat Neurosci 4:499–506.

Garaschuk O, Hanse E, Konnerth A. 1998. Developmental profile and synaptic origin of early network oscillations in the CA1 region of rat neonatal hippocampus. J Physiol 507.1:219–236.

Groc L, Petanjek Z, Gustafsson B, Ben-Ari Y, Hanse E, Khazipov R. 2002. In vivo blockade of neural activity alters dendritic development of neonatal CA1 pyramidal cells. Eur J Neurosci 16:1931–1938.

Guzowski JF. 2002. Insights into immediate-early gene function in hippocampal memory consolidation using antisense oligonucleotide and fluorescent imaging approaches. Hippocampus 12:86–104.

Guzowski JF, McNaughton BL, Barnes CA, Worley PF. 1999. Environment-specific expression of the immediate-early gene Arc in hippocampal neuronal ensembles. Nat Neurosci 2:1120–1124.

Guzowski JF, Timlin JA, Roysam B, McNaughton BL, Worley PF, Barnes CA. 2005. Mapping behaviorally relevant neural circuits with immediate-early gene expression. Curr Opin Neurobiol 15: 599–606.

Harris KM, Teyler TJ. 1984. Developmental onset of long-term potentiation in area CA1 of the rat hippocampus. J Physiol 346: 27–48.

Hu JH, Park JM, Park S, Xiao B, Dehoff MH, Kim S, Hayashi T, Schwarz MK, Huganir RL, Seeburg PH, Linden DJ, Worley PF. 2010. Homeostatic scaling requires group 1 mGluR activation mediated by Homer1a. Neuron 68:1128–1142.

Inoue Y, Udo H, Inokuchi K, Sugiyama H. 2007. Homer1a regulates the activity-induced remodeling of synaptic structures in cultured hippocampal neurons. Neuroscience 150:841–852.

Jaubert PJ, Golub MS, Lo YY, Germann SL, Dehoff MH, Worley PF, Kang SH, Schwarz MK, Seeburg PH, Berman RF. 2007. Complex, multimodal behavioral profile of Homer1 knockout mouse. Genes Brain Behav 6:141–154.

Jones SP, Rahimi O, O'Boyle MP, Diaz DL, Claiborne BJ. 2003. Maturation of granule cell dendrites after mossy fiber arrival in hippocampal field CA3. Hippocampus 13:413–427.

Kato A, Ozawa F, Saitoh Y, Fukazawa Y, Sugiyama H, Inokuchi K. 1998. Novel members of the Vesl/Homer family of PDZ proteins that bind metabotropic glutamate receptors. J Biol Chem 273: 23969–23975.

Kato A, Ozawa F, Saitoh Y, Hirai K, Inokuchi K. 1997. vesl, a gene encoding VASP/Ena family related protein, is upregulated during seizure, long-term potentiation and synaptogenesis. FEBS Lett 412: 183–189.

Khazipov R, Khalilov I, Tyzio R, Morozova E, Ben-Ari Y, Holmes GL. 2004. Developmental changes in GABAergic actions and seizure susceptibility in the rat hippocampus. Eur J Neurosci 19:590–600.

Kirov SA, Goddard CA, Harris KM. 2004. Age-dependence in the homeostatic upregulation of hippocampal dendritic spine number during blocked synaptic transmission. Neuropharmacology 47: 640–648.

Kubik S, Miyashita T, Guzowski JF. 2007. Using immediate-early genes to map hippocampal subregional functions. Learn Mem 14: 758–770.

Langston RF, Ainge JA, Couey JJ, Canto CB, Bjerknes TL, Witter MP, Moser EI, Moser MB. 2010. Development of the spatial representation system in the rat. Science 328:1576–1580.

Li Y, Popko J, Krogh KA, Thayer SA. 2013. Epileptiform stimulus increases Homer 1a expression to modulate synapse number and activity in hippocampal cultures. J Neurophysiol 109:1494–1504.

Lominac KD, Oleson EB, Pava M, Klugmann M, Schwarz MK, Seeburg PH, During MJ, Worley PF, Kalivas PW, Szumlinski KK. 2005. Distinct roles for different Homer1 isoforms in behaviors and associated prefrontal cortex function. J Neurosci 25:11586–11594.

Lu B, Wang KH, Nose A. 2009. Molecular mechanisms underlying neural circuit formation. Curr Opin Neurobiol 19:162–167.

Lu Q, McNaughton BL. 2010. Towards large scale image acquisition and fully automated quantification of activity induced IEG expression in central nervous system. Program No. 204.21. Neuroscience Meeting Planner. San Diego, CA: Society for Neuroscience, 2010.

Maffei A, Turrigiano G. 2008. The age of plasticity: Developmental regulation of synaptic plasticity in neocortical microcircuits. Prog Brain Res 169:211–223.

Maret S, Dorsaz S, Gurcel L, Pradervand S, Petit B, Pfister C, Hagenbuchle O, O'Hara BF, Franken P, Tafti M. 2007. Homer1a is a core brain molecular correlate of sleep loss. Proc Natl Acad Sci USA 104:20090–20095.

Marrone DF, Schaner MJ, McNaughton BL, Worley PF, Barnes CA. 2008. Immediate-early gene expression at rest recapitulates recent experience. J Neurosci 28:1030–1033.

McAllister AK. 2007. Dynamic aspects of CNS synapse formation. Annu Rev Neurosci 30:425–450.

McNaughton BL, Navratilova Z, Burke SN, Barnes CA. 2007. Delayed onset of post-natal expression of plasticity related immediate early gene Arc in medial entorhinal cortex grid cell network. Program No. 744.2. Neuroscience Meeting Planner. San Diego, CA: Society for Neuroscience, 2007.

Miyashita T, Kubik S, Haghighi N, Steward O, Guzowski JF. 2009. Rapid activation of plasticity-associated gene transcription in hippocampal neurons provides a mechanism for encoding of one-trial experience. J Neurosci 29:898–906.

Nosyreva ED, Huber KM. 2005. Developmental switch in synaptic mechanisms of hippocampal metabotropic glutamate receptor-dependent long-term depression. J Neurosci 25:2992–3001.

O'Donovan MJ. 1999. The origin of spontaneous activity in developing networks of the vertebrate nervous system. Curr Opin Neurobiol 9:94–104.

Pawley J. 2006. Handbook of Biological Confocal Microscopy, 3rd ed. NY: Springer Science+Business Media, LLC.

Paxinos G and Watson C. 2007. The Rat Brain in Stereotaxic Coordinates, 6th ed. Amsterdam: Elsevier, Academic Press.

Penner MR, Roth TL, Chawla MK, Hoang LT, Roth ED, Lubin FD, Sweatt JD, Worley PF, Barnes CA. 2011. Age-related changes in Arc transcription and DNA methylation within the hippocampus. Neurobiol Aging 32:2198–2210.

Rahimi O, Claiborne BJ. 2007. Morphological development and maturation of granule neuron dendrites in the rat dentate gyrus. Prog Brain Res 163:167–181.

Rao A, Kim E, Sheng M, Craig AM. 1998. Heterogeneity in the molecular composition of excitatory postsynaptic sites during development of hippocampal neurons in culture. J Neurosci 18: 1217–1229.

Sala C, Futai K, Yamamoto K, Worley PF, Hayashi Y, Sheng M. 2003. Inhibition of dendritic spine morphogenesis and synaptic transmission by activity-induce protein Homer 1a. J Neurosci 23: 6327–6337.

Schreiber SS, Tocco G, Najm L, Finch CE, Johnson SA, Baudry M. 1992. Absence of c-fos induction in neonatal rat brain after seizures. Neurosci Lett 136:31–35.

Shiraishi Y, Mizutani A, Mikoshiba K, Furuichi T. 2003. Coincidence in dendritic clustering and synaptic targeting of homer proteins and NMDA receptor complex proteins NR2B and PSD95 during development of cultured hippocampal neurons. Mol Cell Neurosci 22:188–201.

Storey TW,Storey TW, Rho JM, White SS, Sankar R, Szot P. 2002. Age-dependent differences in flurothyl-induced c-fos and c-jun mRNA expression in the mouse brain. Dev Neurosci 24:294–299.

Sutor B, Luhmann HJ. 1995. Development of excitatory and inhibitory postsynaptic potential in the rat neocortex. Perspect Dev Neurobiol 2:409–419.

Szumlinski KK, Lominac KD, Kleschen MJ, Oleson EB, Dehoff MH, Schwarz MK, Seeburg PH, Worley PF, Kalivas PW. 2005. Behavioral and neurochemical phenotyping of Homer1 mutant mice: Possible relevance to schizophrenia. Genes Brain Behav 4:273–288.

Tyzio R, Holmes GL, Ben-Ari Y, Khazipov R. 2007. Timing of developmental switch in GABA(A) mediated signaling from excitation to inhibition in CA3 rat hippocampus using gramicidin perforated patch and extracellular recordings. Epilepsia 48 (Suppl 5):986-100.

Vazdarjanova A, Guzowski JF. 2004. Differences in hippocampal neuronal population responses to modification of an environmental context: Evidence for distinct, yet complementary, functions of CA3 and CA1 ensembles. J Neurosci 22:10067–10071.

Vazdarjanova A, McNaughton BL, Barnes CA, Worley PF, Guzowski JF. 2002. Experience-dependent coincident expression of the effector immediate-early genes arc and Homer1a in hippocampal and neocortical neuronal networks. J Neurosci 22:10067–10071.

Vendrell M, Curran T, Morgan JI. 1998. A gene expression approach to mapping the functional maturation of the hippocampus. Brain Res Mol Brain Res 63:25–34.

Wills TJ, Cacucci F, Burgess N, O'Keefe J. 2010. Development of the hippocampal cognitive map in preweanling rats. Science 328: 1573–1576.

Witharana WL, Trivedi V, McNaughton BL. 2011. Homer1a intranuclear foic vary in size and intensity depending on behavioral conditions, but not on hippocampal subregions. Program No. 937.23. Neuroscience Meeting Planner. Washington, DC: Society for Neuroscience, 2011.

Worley PF, Zeng W, Huang G, Kim JY, Shin DM, Kim MS, Yuan JP, Kiselyov K, Muallem S. 2007. Homer proteins in Ca2+ signalling by excitable and non excitable cells. Cell Calcium 42:363–371.

Ye GL, Song Liu X, Pasternak JF, Trommer BL. 2000. Maturation of glutamatergic neurotransmission in dentate gyrus granule cells. Brain Res Dev Brain Res 124:33–42.

Yoshihara Y, De Roo M, Muller D. 2009. Dendritic spine formation and stabilization. Curr Opin Neurobiol 19:146–153.